Journal of Solid State Chemistry 184 (2011) 2840–2848

Contents lists available at SciVerse ScienceDirect

Journal of Solid State Chemistry

journal homepage: www.elsevier.com/locate/jssc

The system Ce–Zn–B at 800 °C

Z. Malik [a], O. Sologub [a], G. Giester [b], P. Rogl [a,*]

[a] Department of Physical Chemistry, University of Vienna, Waehringerstrasse 42, A-1090 Vienna, Austria
[b] Institute of Mineralogy and Crystallography, University of Vienna, Althanstrasse 14, A-1090 Vienna, Austria

ARTICLE INFO

Article history:
Received 1 July 2011
Received in revised form
10 August 2011
Accepted 14 August 2011
Available online 23 August 2011

Keywords:
Ce–Zn–B phase diagram
Ce–Zn system
Crystal structure
Ce_3Zn_{11}
Ce_3Zn_{22}

ABSTRACT

The isothermal section for the system Ce–Zn–B has been established at 800 °C using electron microprobe analysis and X-ray powder diffraction. No ternary compounds exist and mutual solid solubilities of binary phases are negligible. In the concentration range of 10.0–10.5 at% Ce two structural modifications have been confirmed: high temperature βCe_2Zn_{17} above ~750 °C with the Th_2Zn_{17} type ($R\bar{3}m$, a=0.90916(4) nm, c=1.3286(1) nm) and low temperature $\alpha CeZn_7$ ($Ce_{1-x}Zn_{5+2x}$; x~0.33) up to 750 °C for which we attributed the $TbCu_7$ type ($P6/mmm$, a=0.52424(2), c=0.44274(1) nm). The crystal structure of $CeZn_7$ was derived from the Rietveld refinement of X-ray powder intensities. Precise data on atom site distribution and positional parameters have been furthermore provided from X-ray single crystal refinements for two compounds, for which crystal structures hitherto have only been derived from X-ray diffraction photographs: Ce_3Zn_{11} ($Immm$, a=0.45242(2) nm, b=0.88942(3) nm, c=1.34754(4) nm) and Ce_3Zn_{22} ($I4_1/amd$; a=0.89363(2) nm, c=2.1804(5) nm).

1. Introduction

Zinc-based alloys with rare-earth metals are used in several engineering applications and are often employed to replace cast iron because of similar properties and better machinability [1]. Rare earths (RE) improve the mechanical performance, tensile strength, hardness and also the corrosion resistance by removing impurities from the grain boundaries of their alloys with zinc [2]. Zinc alloys with about 15 mass% boron or even less exhibit high tensile strength, high degree of hardness, high resistance to oxidation and corrosion, low shrinkage factor and low specific gravity [3]. Multi-component zinc and boron alloys containing various amounts of elements such as aluminium, copper or calcium can be used for the production of bearings, bars, rods, sheets, tubes, plates, for the production of ingots, or other finished or semi-finished articles [3].

As far as high strength lightweight alloys for automotive applications are concerned [4], the Ce–Zn system is an important part of the multinary Mg-based alloy system Mg–Zn–Mn–RE, however, nothing is yet known on the influence of boron additions and no phase diagrams have yet been reported for systems RE–Zn–B. Therefore the present work tries to provide detailed information on phase equilibria and crystal structures in the Ce–Zn–B system.

2. Experimental

Samples in a total amount of ca. 0.5 g each were prepared from cerium ingots (Alfa Aesar, purity > 99.9mass%), zinc granules (Alfa Aesar, purity > 99.9mass%) and boron pieces (ChemPur, Karlsruhe, purity 98mass%). Zinc drops were purified in an evacuated quartz tube by heating them below the boiling temperature of Zn (907 °C). Cerium was mechanically surface cleaned before use.

2.1. Binary alloys

Ce cuttings and Zn filings in various stiochiometric ratios were cold pressed, sealed in quartz tubes under vacuum and then slowly heated to 420 °C. Samples were kept at this temperature for 12 h before heating up to the melting range (about 100 °C above T_m) at the rate of 1 °C/min prior to cooling down to 800 °C at the same rate. The reguli were annealed at 800 °C for 7 days and quenched by immersing the quartz ampoules in cold water. Selected alloys were annealed at various temperatures in the range of 420 °C–850 °C for 7 days. CeB_6 and CeB_x master alloys were prepared by arc melting cerium cuttings and boron pieces under argon.

2.2. Ternary alloys

Two procedures were used for the evaluation of ternary phase relations:

(i) samples were prepared from intimate blends of powders of arcmelted CeB_x master alloy and fine Zn-filings in proper

* Corresponding author.
E-mail address: peter.franz.rogl@univie.ac.at (P. Rogl).

0022-4596/$ - see front matter © 2011 Elsevier Inc. All rights reserved.
doi:10.1016/j.jssc.2011.08.020

compositional ratios. The blends were cold compacted in a steel die without lubricant, vacuum sealed in quartz tubes and heat treated and quenched as described for the binary alloys.

(ii) samples were prepared from mixtures of arcmelted CeB_6 and binary Ce_xZn_y master alloys prepared like described in (i). Melting and heat treatment was performed as for alloys (i).

X-ray powder diffraction data were collected from each alloy in as cast and annealed state employing a Guinier–Huber image plate system with monochromatic Cu$K\alpha_1$ radiation ($8^\circ < 2\theta < 100^\circ$). Quantitative Rietveld refinements of the X-ray powder diffraction data were performed with the FULLPROF program [5].

Single crystals were mechanically isolated from crushed as cast alloys. Inspections on an AXS-GADDS texture goniometer

Table 1
Crystallographic data of unary and binary boundary solid phases of the system Ce–Zn–B.

Phase, temperature range (°C)	Space group, prototype	Lattice parameters (nm)			Comments
		a	*b*	*c*	
(δCe) 798–700 [10]	$Im\bar{3}m$ W	0.412		–	[10] $0 \le x \le 0.014$ at 722 °C [10]
(γCe) < 726 [10]	$Fm\bar{3}m$ Cu	0.51610		–	[10]
(Zn) < 420	$P6_3/mmm$ Mg	0.2665 0.2667(1)		0.4947 0.4951(1)	[10] From alloy Ce7Zn93, 600 °C[a]
(βB) < 2092 [10] Zn_xB_{1-x}	$R\bar{3}m$ βB –	1.09251 – – 1.093 1.100 1.0986(2)	– 	2.38143 – – 2.374 2.404 2.4016(4)	[13] – $0 \le x \le 0.042$ at 907 °C [29] $x=0$ at 907 °C [29] $x=0.042$ at 907 °C [29] $x=0.039$ at 907 °C [30]
CeZn < 825 [10]	$Pm\bar{3}m$ CsCl	0.3704(1) 0.37125(2) 0.37059(2)			[13] 850 °C [This work][a] 830 °C Ce poor [This work][a]
$CeZn_2$ < 875 [10]	*Immm* $CeCu_2$	0.4633(5) 0.46393(8) 0.46356(4)	0.7538(5) 0.7544(1) 0.75375(7)	0.7499(5) 0.7506(1) 0.75525(6)	[13] 700 °C Ce-rich [This work][a] 850 °C Ce-poor [This work][a]
$CeZn_3$ < 820 [10]	*Cmcm* $CeZn_3$	0.4620(5) 0.46324(5) 0.4635(1)	1.0440(5) 1.0452(1) 1.0439(3)	0.6640(5) 0.66557(6) 0.6641(2)	[13] 850 °C Ce-rich [This work][a] 850 °C Ce-poor [This work][a]
Ce_3Zn_{11} < 840 [10]	*Immm* La_3Al_{11}	0.45215 0.45242(2) 0.45222(1) 0.45175(6)	0.88855 0.88942(3) 0.88898(2) 0.8894(1)	1.3463 1.34754(4) 1.34649(4) 1.3447(2)	[13] Single crystal [This work] 820 °C Ce-rich [This work][a] 820 °C Ce-poor [This work][a]
$Ce_{13}Zn_{58}$ < 870 [10]	$P6_3/mmc$ $Gd_{13}Zn_{58}$	1.4638(1) 1.4616(1) 1.4635(5)		1.4158(1) 1.4173(1) 1.4176(5)	820 °C[c] [19] 820 °C Ce-rich [This work][a] 820 °C [This work][a]
$CeZn_5$ < 885 [10] $CeZn_{5+y}$	$P6/mmm$ $CaCu_5$	0.54163(5) 0.54082(1) 0.54163(5)		0.42647(5) 0.42798(1) 0.42647(5)	[13] 800 °C Ce poor [This work][a] $0.017 \le y \le 0.046$ < 885 °C [16]
Ce_3Zn_{22} < 960 [10]	$I4_1/amd$ Ce_3Zn_{22}	0.897(1) 0.8936(2) 0.89331(2) 0.89286(1)		2.133(5) 2.1380(5) 2.13701(6) 2.13599(2)	[17] Single crystal [This work] 800 °C Ce-rich [This work][a] 850 °C Ce-poor [This work][a]
β Ce_2Zn_{17} < 980 [10] 980-~750 [This Work]	$R\bar{3}m$ Th_2Zn_{17}	0.9090(5) 0.90916(4) 0.90884(7) 0.90947(1)		1.32844(7) 1.32861(1) 1.3300(1) 1.32955(2)	827 °C [13] 850 °C [This work][a] 850 °C Ce-rich [This work][a] 750 °C Ce-poor [This work][a]
α Ce_2Zn_{17} < ~750[This work]	$P6_3/mmc$ Th_2Ni_{17} $TbCu_7$	0.9088(4) 0.52424(2)		0.8856(5) 0.44274(1)	[21] 700 °C [This work][a]
$CeZn_{11}$ < 795 [10]	$I4_1/amd$ $BaCd_{11}$	1.0658(6) 1.06630(1) 1.0666(1) 1.06689(2)		0.6862(8) 0.686644(7) 0.68645(1) 0.68680(2)	497 °C [15] 480 °C [This work][a] 600 °C Ce rich [This work][a] 600 °C Ce poor [This work][a]
CeB_4 < 2380 [10] < 2165 [14]	$P4/mbm$ UB_4	0.7208(1)		0.4091(1)	[13]
CeB_6 < 2550 [10] < 2330 [14]	$Pm\bar{3}m$ CaB_6	0.4139(4)			[13]

[a] Quenching temperature of samples while the lattice parameters are measured at room temperature.

assured high crystal quality, unit cell dimensions and Laue symmetry of the specimens prior to the X-ray intensity data collections on a four-circle Nonius Kappa diffractometer equipped with a CCD area detector employing graphite monochromated Mo $K\alpha$ radiation ($\lambda = 0.071069$ nm). Orientation matrices and unit cell parameters were derived using the program DENZO [6]. No absorption corrections were performed because of the rather regular crystal shapes and small dimensions of the investigated specimens. The structures were solved by direct methods and were refined with the SHELXL-97 program [7,8] within the Windows version WINGX [9]. The as cast and annealed samples were polished using standard procedures and microstructures and compositions were examined by light optical microscopy (LOM) and scanning electron microscopy (SEM) via Electron Probe Micro-Analyses (EPMA) on a Zeiss Supra 55 VP equipped with an EDX system operated at 20 kV. For binary compounds βCe_2Zn_{17} was used as EPMA standard. The differences between measured and nominal compositions were found to be < 1 at%.

Table 2a
Crystal structure data[a] from X-ray single crystal evaluation of Ce_3Zn_{11} and Ce_3Zn_{22}.

Compound	**Ce_3Zn_{11}**	**Ce_3Zn_{22}**
Composition (at. %)[c]	$Ce_{23.35}Zn_{76.65}$	$Ce_{12}Zn_{88}$
Space group	*Immm*; No. 71	$I4_1/amd$; No. 141, origin at $\bar{1}$
Structure type	La_3Al_{11}	Ce_3Zn_{22}
Formula from refinement	Ce_3Zn_{11}	Ce_3Zn_{22}
θ Range (deg)	$2.74 < \theta < 36.16$	$2.47 < \theta < 36.26$
Crystal size (μm)	$20 \times 30 \times 45$	$25 \times 30 \times 45$
a (nm)	0.45242(2)	0.89363(2)
b (nm)	0.88942(3)	0.89363(2)
c (nm)	1.34754(4)	2.13804(5)
Reflections in refinement	615 $F_o > 4\sigma(F_o)$ of 759	875 $F_o > 4\sigma(F_o)$ of 1131
Mosaicity	0.55	0.6
Number of variables	28	39
$R_F^2 = \Sigma\lvert F_0^2 - F_c^2\rvert / \Sigma F_0^2$	0.026	0.021
R_{Int}	5.6	6.7
GOF	1.059	1.061
Extinction (Zachariasen)	0.0009(1)	0.00011(1)
M1; Occ.	2*a* (0, 0, 0); 1.00 Ce2	8*e*(0, ¼, *z*); $z = 0.25343(2)$; 1.00 Ce1
U_{11}; U_{22}; U_{33}; U_{23}; U_{13}; U_{12}[b]	0.0139(3); 0.0239(3); 0.0096(2); 0; 0; 0	0.0084(1); 0.0065(1); 0.0076(1); 0; 0; 0
M2; Occ.	4*i* (0, 0, *z*); $z = 0.29571(2)$; 1.00 Ce1	4*a* (0, $^3/_4$, 1/8); 1.00 Ce2
U_{11}; U_{22}; U_{33}; U_{23}; U_{13}; U_{12}[b]	0.0089(2); 0.0103(2); 0.0103(2); 0; 0; 0	0.0066(1); 0.006(1); 0.0069(1); 0; 0; 0
M3; Occ.	8*l* (0, *y*, *z*); $y = 0.35869(7)$, $z = 0.34366(4)$; 1.00 Zn2	32*i* (*x*, *y*, *z*); $x = 0.23223(4)$, $y = 0.00749(4)$, $z = 0.1889(2)$; 1.00 Zn1
U_{11}; U_{22}; U_{33}; U_{23}; U_{13}; U_{12}[b]	0.0119(3); 0.0109(3); 0.0166(3); 0; 0.002(2); 0	0.0122(2); 0.0111(2); 0.0096(2); 0.0017(1); 0.0002(1); 0.0009(1)
M4; Occ.	8*l* (0, *y*, *z*); $y = 0.28363(7)$, $z = 0.14007(4)$; 1.00 Zn1	16*h* (0, *y*, *z*) $y = 0.02584(6)$, $z = 0.37681(2)$; 1.00 Zn2
U_{11}; U_{22}; U_{33}; U_{23}; U_{13}; U_{12}[b]	0.0107(3); 0.0144(3); 0.0211(3); -0.0006(2); 0	0.0091(2); 0.0147(2); 0.0119(2); -0.0021(2); 0; 0;
M5; Occ.	4*h* (0, *y*, ½); $y = 0.18232(10)$; 1.00 Zn3	16*h* (0, *y*, *z*) $y = 0.10292(6)$, $z = 0.11676(2)$; 1.00 Zn3
U_{11}; U_{22}; U_{33};U_{23}; U_{13}; U_{12}[b]	0.0193(4); 0.0180(4); 0.0118(3); 0; 0; 0	0.0112(2); 0.0094(2); 0.0114(2); -0. 0012(2); 0; 0;
M6; Occ.	2*d* (½, 0, ½); 1.00 Zn4	16*h* (0, *y*, *z*) $y = 0.59875(6)$; $z = 0.26315(2)$; 1.00 Zn4
U_{11}; U_{22}; U_{33}; U_{23}; U_{13}; U_{12}[b]	0.0187(6); 0.0187(6); 0.0173(5); 0; 0; 0	0.0092(2); 0.0099(2); 0.0130(2); 0. 0017(2); 0; 0;
M7; Occ.		8*c* (0, 0, 0); 1.00 Zn5
U_{11}; U_{22}; U_{33}; U_{23}; U_{13}; U_{12}[b]		0.0083(3); 0.0104(3); 0.0111(3); -0.0021(3); 0; 0
Residual electron density; max; min in [electrons/nm^3] $\times 10^3$	2.83; –1.85	2.37; –1.33

[a] Crystal structure data are standardized using the program Structure Tidy [31].
[b] Anisotropic atomic displacement parameters U_{ij} in (10^2 nm^2).
[c] Nominal composition of the alloy from which a single crystal was isolated.

Table 2b
Interatomic distances in Ce_3Zn_{11}.

Atom	Distance (nm)	Atom	Distance (nm)	Atom	Distance (nm)
Ce1–4Zn1	0.30935(4)	Zn1–2Zn2	0.26014(4)	Zn3–2Zn2	0.26266(7)
Ce1–2Zn3	0.31950(5)	Zn1–Zn4	0.26956(6)	Zn3–2Zn4	0.27833(5)
Ce1–4Zn2	0.31975(4)	Zn1–Zn2	0.28236(7)	Zn3–4Zn1	0.29616(4)
Ce1–2Zn2	0.32550(6)	Zn1–2Zn3	0.29616(4)	Zn3–Zn3	0.32432(13)
Ce1–2Zn1	0.32806(6)	Zn1–2Ce1	0.30935(4)	Zn3–2Ce1	0.31950(5)
Ce1–2Zn4	0.35631(3)	Zn1–Ce2	0.31506(6)	Zn3–2Ce2	0.36195(7)
Ce1–Ce2	0.39848(3)	Zn1–Ce1	0.32807(6)	Zn4–4Zn1	0.26956(6)
Ce2–4Zn1	0.31506(6)	Zn2–Zn2	0.25137(12)	Zn4–4Zn3	0.27833(5)
Ce2–8Zn2	0.33369(4)	Zn2–2Zn1	0.26014(4)	Zn4–4Ce1	0.35631(3)
Ce2–4Zn3	0.36195(7)	Zn2–Zn3	0.26266(7)		
Ce2–2Ce1	0.39848(3)	Zn2–Zn1	0.28236(7)		
		Zn2–2Ce1	0.31975(4)		
		Zn2–Ce1	0.32550(6)		
		Zn2–2Ce2	0.33369(4)		

3. Results and discussion

3.1. Binary boundary systems

The binary systems Zn–B and Ce–B were used in the version presented by Massalski [10]. In agreement with literature data, we observed no evidence of chemical interaction between zinc and boron. The formation and crystal structures of compounds CeB_4 and CeB_6 were confirmed. Although several critical assessments have been recently published on the phases and phase relations in the Ce–Zn binary [11,12], our work on the ternary Ce–Zn–B system revealed several structural inconsistencies for the binary Ce–Zn compounds [10,13,14], which made a reinvestigation of the crystal structures in the Ce–Zn binary system necessary (see below).

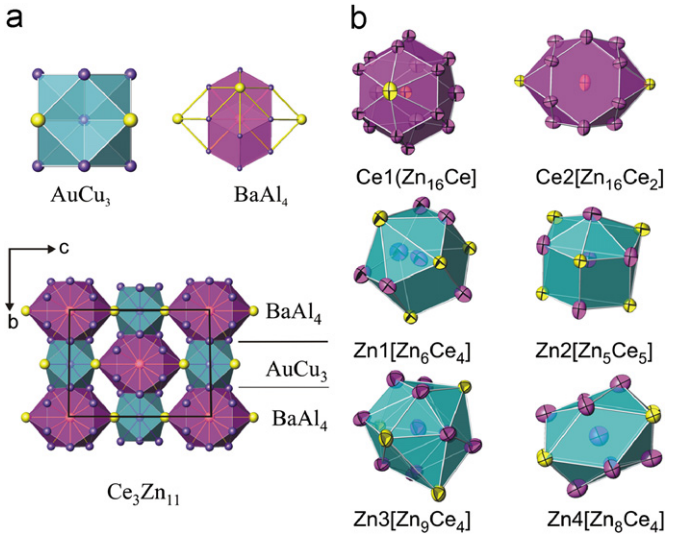

Fig. 1. (a) Crystal structure of Ce_3Zn_{11} (La_3Al_{11}-type) as an arrangement of building blocks of $AuCu_3$-and $BaAl_4$-type and (b) Coordination polyhedra for all crystallographic sites in Ce_3Zn_{11} with anisotropic displacement ellipsoids from single crystal refinement.

The crystal data relevant to the unary and binary boundary phases in the Ce–Zn–B system, including results of our reinvestigation of the Ce–Zn system, are presented in Table 1.

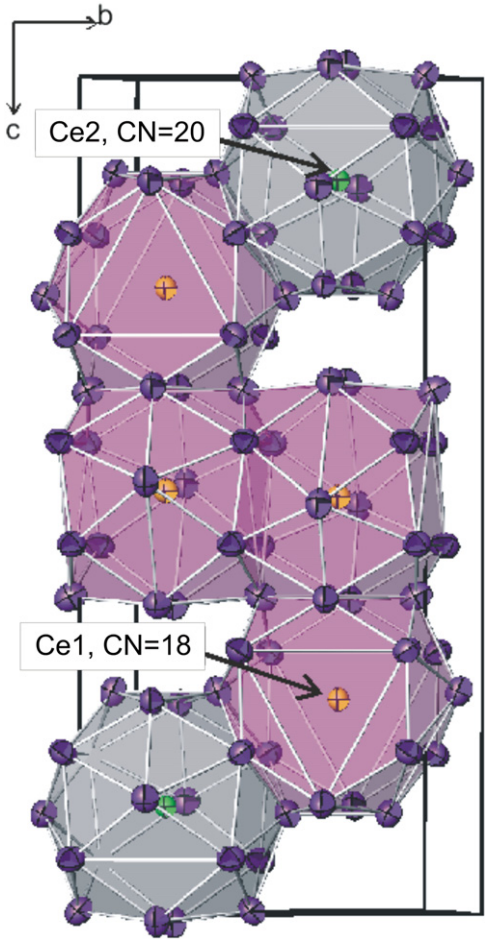

Fig. 2. Unit cell of Ce_3Zn_{22} revealing the coordination polyhedra around atom sites for Ce1 and Ce2. Anisotropic displacement parameters comply with single crystal refinement.

Table 2c
Interatomic distances in Ce_3Zn_{22}.

Atom	Distance (nm)	Atom	Distance (nm)	Atom	Distance (nm)
Ce1–2Zn4	0.3124(1)	Zn2–2Zn1	0.2571(1)	Zn4–2Zn5	0.2626(1)
Ce1–2Zn3	0.3204(1)	Zn2–Zn4	0.2673(1)	Zn4–Zn2	0.2673(1)
Ce1–2Zn2	0.3251(1)	Zn2–2Zn1	0.2779(1)	Zn4–Zn4	0.2703(1)
Ce1–4Zn1	0.3303(1)	Zn2–2Zn3	0.2802(1)	Zn4–2Zn1	0.2771(1)
Ce1–2Zn2	0.3312(1)	Zn2–2Zn2	0.2834(1)	Zn4–2Zn1	0.2780(1)
Ce1–4Zn1	0.3456(1)	Zn2–Ce1	0.3251(1)	Zn4–2Zn3	0.2909(1)
Ce1–2Zn2	0.3661(1)	Zn2–Ce1	0.3312(1)	Zn4–Ce1	0.3123(1)
Ce2–4Zn3	0.3159(1)	Zn2–Ce1	0.3661(1)	Zn4–Ce2	0.3218(1)
Ce2–4Zn4	0.3248(1)	Zn3–Zn3	0.2629(1)	Zn4–Zn3	0.3611(1)
Ce2–8Zn1	0.3386(1)	Zn3–Zn5	0.2660(1)	Zn5–4Zn4	0.2626(1)
Ce2–4Zn5	0.3483(1)	Zn3–2Zn1	0.2722(1)	Zn5–4Zn1	0.2651(1)
Zn1–Zn2	0.2571(1)	Zn3–2Zn2	0.2802(1)	Zn5–2Zn3	0.2660(1)
Zn1–Zn1	0.2633(1)	Zn3–2Zn1	0.2806(1)	Zn5–2Ce2	0.3483(1)
Zn1–Zn5	0.2651(1)	Zn3–2Zn4	0.2909(1)		
Zn1–Zn3	0.2722(1)	Zn3–Ce2	0.3158(1)		
Zn1–Zn1	0.2750(1)	Zn3–Ce1	0.3204(1)		
Zn1–Zn4	0.2771(1)	Zn3–Zn4	0.3611(1)		
Zn1–Zn2	0.2779(1)				
Zn1–Zn4	0.2780(1)				
Zn1–Zn3	0.2805(1)				
Zn1–Ce1	0.3303(1)				
Zn1–Ce2	0.3386(1)				
Zn1–Ce1	0.3456(1)				

3.2. The system Ce–Zn

Crystal structure Rietveld refinements for all those binary compounds, which have been already reported earlier, namely $CeZn_{11}$ [15], $CeZn_5$, $CeZn_3$, $CeZn_2$ and CeZn [10,13], were found to be consistent with data in the literature. Therefore, the reinvestigation of crystal structures and phase relations in the Ce–Zn system essentially focused on the determination of crystal symmetry, precise atom site distribution and positional parameters for those compounds (*hexagonal*-$CeZn_{\sim 7}$, *rhombohedral*-Ce_2Zn_{17}, Ce_3Zn_{22}, $Ce_{13}Zn_{58}$, and Ce_3Zn_{11}), for which crystal structure data hitherto have only been derived from X-ray diffraction photographs or have not been evaluated (*hex*-$CeZn_{\sim 7}$).

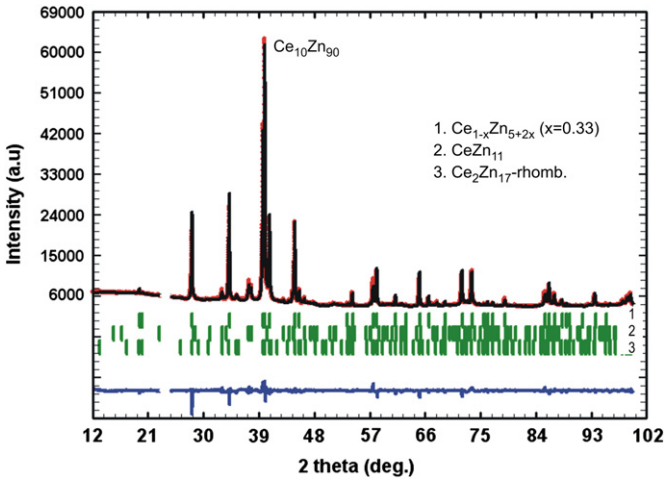

Fig. 3. X-ray powder spectrum of alloy $Ce_{10}Zn_{90}$ and Rietveld refinement of the low temperature phase: hexagonal $CeZn_7$ ($Ce_{1-x}Zn_{5+2x}$, $x=0.33$) with $TbCu_7$-type. (Excluded region contains a small peak from sample holder).

3.2.1. Structural chemistry

3.2.1.1. X-ray single crystal intensity data refinement of Ce_3Zn_{11} and Ce_3Zn_{22}.

Ce_3Zn_{11}: The X-ray intensity spectrum of a single crystal selected from the crushed sample $Ce_{23.35}Zn_{76.65}$ (at%) was fully indexed with an orthorhombic lattice ($a=0.45242(2)$ nm, $b=0.88942(3)$ nm, $c=1.34754(4)$ nm). Systematic extinctions only observed for a body-centred Bravais lattice (*hkl*), $h+k+l=2n+1$ indicated the space groups *Immm*, *I*222, *Imm*2 and $I2_12_12_1$. *Immm* with highest symmetry was used to solve the crystal structure employing direct methods. Composition, lattice parameters, crystal symmetry, Wyckoff sequence 2*a*, 2*d*, 4*h*, 4*i*, $8l^2$ and atom parameters prompted isotypism with the structure type of La_3Al_{11}. The structure solution converged at $R_{F^2}=2.6$ yielding a residual electron density less than $\pm 2.8\ e^-/Å^3$. Crystal data and interatomic distances are presented in Tables 2a and 2b. The characteristic stacking of face-connected units…$AuCu_3$–$BaAl_4$ …is documented in Fig. 1 including the polyhedra of the individual atom sites. Although the structure solution provides positional and thermal atom parameters of significantly higher precision it confirms the early structure determination of Ce_3Zn_{11} by Lott and Chiotti [16] performed on the basis of X-ray Weissenberg and precession photographs.

Ce_3Zn_{22}: The first analysis of the crystal structure of Ce_3Zn_{22} from essentially steric considerations is due to Kripyakevich et al.

Table 3a
Rietveld refinement data for $Ce_{13}Zn_{58}$, $Ce_{1-x}Zn_{5+2x}$-hex; ($x=0.33$; $\alpha CeZn_7$) and alloy $Ce_{8.6}Zn_{70.7}B_{20.7}$ (all from Guinier – Huber Image Plate, Cu$K\alpha_1$).

Compound	$Ce_{13}Zn_{58}$	$Ce_{1-x}Zn_{5+2x}$-hex; ($x=0.33$)	Ce_2Zn_{17}-rhombohedral
Nominal composition (at%)	$Ce_{18.31}Zn_{81.69}$	$Ce_{10}Zn_{90}$	$Ce_{8.6}Zn_{70.7}B_{20.7}$
Composition from EPMA	$Ce_{18.0}Zn_{82.0}$	–	$Ce_{11.08}Zn_{88.92}$
Space group	$P6_3/mmc$; No. 194	$P6/mmm$; No. 191	$R\bar{3}m$; No. 166
Structure type	$Ce_{13}Zn_{58}$	$TbCu_7$	Th_2Zn_{17}
Composition from refinement	$Ce_{16.3}Zn_{82.7}$	$Ce_{10.6}Zn_{89.4}$	$Ce_{10.5}Zn_{89.5}$
Theta range	$8^\circ < 2\theta < 100^\circ$	$8^\circ < 2\theta < 100^\circ$	$8^\circ < 2\theta < 100^\circ$
a (nm)	1.4616(1)	0.52424(2)	0.90872(1)
c (nm)	1.418(1)	0.44274(1)	1.32825(2)
Reflections in refinement	606	39	146
No. of parameters refined	103	26	39
Reliability factors			
$R_F=\Sigma\lvert F_o-F_c\rvert/\Sigma F_o$	0.032	0.045	0.038
$R_{exp}=[(N-P+C)/\Sigma(w_i y_{oi}^2)]^{1/2}$	0.032	0.035	0.024
$\chi^2=(R_{wP}/R_e)^2$	11.2	5.84	4.15
R1; Occ.; B_{iso}	12*k* (*x*, 2*x*, *z*); $x=0.2031(4)$, $z=0.0529(3)$; 0.888(2) Ce1; 0.85(5)	1*a* (0, 0, 0); 0.67(3) Ce1; 0.29(2)	6*c* (0, 0, *z*); $z=0.33561(7)$; 1.00(1) Ce1; 0.32(2)
R2 in 6*h* (*x*, 2*x*, ¼); Occ.; B_{iso}	$x=0.5057(9)$; 0.448(2) Ce2; 0.4(1)		
R3 in 6*h* (*x*, 2*x*, ¼); Occ.; B_{iso}	$x=0.875(4)$; 0.486(1) Ce3; 0.8(1)		
R4 in 2*a* (0, 0, 0); Occ., B_{iso}	0.924(2)Ce4; 0.7(2)		
M1; Occ.; B_{iso}	24*l* (*x*, *y*, *z*); $x=0.3725(4)$, $y=0.0374(5)$, $z=0.0992(5)$; 0.948(8) Zn1; 0.9(1)	3*g* (½, 0, ½); 1.00(1) Zn1; 0.15(3)	18*h* ($x,\bar{x}$, *z*); $x=0.5052(4)$, $z=0.15512(7)$; 1.00(1) Zn1; 0.20(2)
M2; Occ.; B_{iso}	12*k* (*x*, 2*x*, *z*); $x=0.0923(7)$, $z=0.1548(6)$; 0.868(6) Zn2; 0.9(1)	2*e* (0,0, *z*); $z=0.2995(5)$; 0.33(1) Zn2; 0.43(2)	18*f* (*x*, 0.0); $x=0.29213(9)$; 1.00(1) Zn2; 0.20(3)
M3; Occ.; B_{iso}	12*k* (*x*, 2*x*, *z*); $x=0.247(2)$, $z=0.6724(6)$; 0.858(8) Zn3; 0.8(2)	2*c* ($^1/_3$, $^2/_3$, 0); 1.00(1) Zn3; 0.46(3)	9*d* (½, 0, ½); 1.00(1) Zn3; 0.53(4)
M4; Occ.; B_{iso}	12*k* (*x*, 2*x*, *z*); $x=0.549(2)$, $z=0.6332(7)$; 1.00(1) Zn4; 0.3(2)		6*c* (0.0,*z*); $z=0.0988(1)$; 1.00(1) Zn4; 0.67(4)
M5 in 12*k* (*x*, 2*x*, *z*); Occ., B_{iso}	$x=0.5995(9)$, z=0.0521(7); 1.00(1) Zn5; 0.8(1)		9*e* (½, 0, 0); 0.15(4)B; 0.8(–)
M6 in 12*j* (*x*, *y*, ¼); Occ., B_{iso}	$x=0.0910(7)$, $y=0.3728(7)$; 0.958(5) Zn6; 0.2(1)		
M7 in 12*i* (*x*, 0, 0); Occ., B_{iso}	$x=0.194(3)$; 0.552(5) Zn7; 0.3(3)		
M8 in 6*h* (*x*, 2*x*, ¼); Occ., B_{iso}	$x=0.2701(5)$, 1.00(1) Zn8; 0.4(2)		
M9 in 6*g* (½, 0, 0); Occ., B_{iso}	0.640(4) Zn9; 0.9(3)		
M10 in 4*f* ($^1/_3$, $^2/_3$, *z*); Occ., B_{iso}	$z=0.095(1)$; 0.882(3) Zn10; 0.3(3)		
M11 in 2*d* ($^1/_3$, $^2/_3$, $^3/_4$); Occ., B_{iso}	0.912(2) Zn11; 0.08(48)		
M12 in 2*b* (0, 0, ¼); Occ., B_{iso}	0.924(2) Zn12; 0.3(5)		

[17] providing a set of atom parameters. Johnson and Wood [18] compared observed and calculated X-ray powder data for Ce_3Zn_{22} and reported isotypism with the structure of Pu_3Zn_{22} for which they solved the structure on the basis of single crystal Weissenberg and precession photographs (reliability factor $R_F=0.096$). In order to provide a precise set of atom parameters and to check on defects or random distributions, a full structure determination was performed on a crystal selected from a crushed sample with nominal composition $Ce_{12}Zn_{88}$ (at%). X-ray intensity data depicted systematic extinctions, (*hkl*) for $h+k+l=2n+1$, (*hk*0) for $h,k=2n+1$ and (*hhl*) for $2h+l=4n+1$ prompted space group $I4_1/amd$ as the one with highest symmetry. Structure analysis employing direct methods ended up at $R_{F^2}=2.1$ and residual electron densities less than, $\pm 2.4\ e^-/Å^3$. The refinement with anisotropic ADPs revealed a fully ordered structure without any defect atom sites. Crystal data and interatomic distances are presented in Tables 2a and 2c, respectively. The crystal structure of Ce_3Zn_{22} is shown in Fig. 2 in three-dimensional view on the *bc* plane emphasizing on the interconnectivity of the Ce-centred polyhedra (Ce1 polyhedra with coordination number 18 and Ce_2 polyhedra with coordination number 20). Description of the structure, coordination polyhedra and interatomic distances are consistent with the description earlier presented for isotypic Pu_3Zn_{22} [18].

3.2.1.2. Rietveld refinement of $Ce_{13}Zn_{58}$, rhombohedral βCe_2Zn_{17} (hT) and of hexagonal $\alpha CeZn_7$ (lT).

$Ce_{13}Zn_{58}$: Recently single crystal studies were reported for the $RE_{13}Zn_{58}$ family of hexagonal quasicrystals derived from $Gd_{13}Cd_{58}$ (RE=Ce, Pr, Nd, Sm, Gd, Tb, Dy) [19]. Whereas the Ce and Pr structures were reported to be identical to the prototype, different types of disorder were detected for the other members of the series. Our X-ray powder refinement of $Ce_{13}Zn_{58}$ revealed significant defects for several atom positions e.g. for the sites Ce3, Zn3 and Zn9. With respect to the formation of periodic structures for the later members of the rare earth series, we assume that the structure of $Ce_{13}Zn_{58}$ may exhibit a similar variability in local ordering rendering the general formula $Ce_{13}Zn_{58}$.

Rhombohedral βCe_2Zn_{17}: Polymorphism was reported for the compound Ce_2Zn_{17} with a rhombohedral structure at high temperatures but a hexagonal structure at low temperature [20,21]. In agreement with the findings in the literature our X-ray powder spectra obtained from samples annealed at 800 °C were fully indexed on the basis of a rhombohedral lattice ($a=0.90916(4)$ nm, $c=1.3286(1)$ nm) prompting isotypism with the structure type of Th_2Zn_{17} (space group $R\bar{3}m$; No. 166). The results of the Rietveld refinement confirm the Th_2Zn_{17}–type as defined earlier for a single crystal study of the high temperature modification of Ce_2Zn_{17} [22].

Hexagonal $\alpha CeZn_7$ (αCe_2Zn_{17}): As already observed by Iandelli and Palenzona [21], it seems extremely difficult to obtain the low temperature form from the high temperature modification (βCe_2Zn_{17}) by long term annealing at 500 °C. βCe_2Zn_{17} however, can easily be formed by heating the low temperature modification above ~775 °C. Slow heating of the mixture of components $Ce_{10.5}Zn_{89.5}$ (at%) up to 500 °C and annealing at this temperature for 5 days produced an alloy with an X-ray powder diffraction pattern yielding a majority of the low-temperature phase. Although the X-ray pattern was completely indexed with an hexagonal cell ($a=0.52424(2)$ nm, $c=0.44274(1)$ nm) for the low temperature form and small amounts of βCe_2Zn_{17} ($P6_3/mmc$) and $CeZn_{11}$ ($BaCd_{11}$-type), the small unit cell parameters do not correspond to the Th_2Ni_{17}-type structure as reported for "αCe_2Zn_{17}" by Iandelli and Palenzona [21] and Veleckis et al. [23]. Much better correspondence between the observed and calculated X-ray powder diffraction patterns was achieved applying the atomic model of the $TbCu_7$ type structure [24]. The $TbCu_7$-type adopts the $CaCu_5$-type unit cell and is a member of a structure family $A_{1-s}B_{5+2s}$ where a fraction s of the A-atoms is randomly or in ordered fashion replaced by a dumbbell of B-atoms covering a range of stoichiometries AB_5 to $AB_{9.5}$ [25]. Rietveld refinement of the "αCe_2Zn_{17}" pattern on the basis of this model prompted a low residual value $R_F=0.045$ with a random distribution of 0.67 Ce in the 1*a* site of space group *P*6/*mmm*, the holes around the vacancies being filled by 0.33 Zn-dumbbells (Zn2) in site 2*e*. Accordingly the overall formula is close to $Ce_{0.7}Zn_{5.6}$ ($Ce_{1-x}Zn_{5+2x}$; $x\sim 0.33$).

The Rietveld refinement profile for $\alpha CeZn_7$ is shown in Fig. 3. Interatomic distances are depicted in Table 3a, 3b and Fig. 4a. A Fourier map (Fig. 5b) shows the presence of the electron density, which refers to the Zn2 atoms. Formally short distances $d_{Ce-Zn2}=0.133$ nm and $d_{Zn2-Zn2}=0.174$ nm appear for the random occupation of Ce and Zn2 atoms. However, either a Ce-atom or a Zn2-dumbbell may exist with an acceptable distance $d_{Ce-Zn2}=0.300$ nm and $d_{Zn2-Zn2}=0.260$ nm.

Table 3b
Interatomic distances for $Ce_{1-x}Zn_{5+2x}$-*hex*; ($x=0.33$).

Atom	Distance (nm)	Atom	Distance (nm)
Ce1–2Zn2	0.13234	Zn2–Ce1	0.13234
Ce1–6Zn3	0.30258	Zn2–Zn2	0.17793
Ce1–2Zn2	0.31027	Zn2–Zn2	0.26468
Ce1 –12Zn1	0.34299	Zn2–6Zn1	0.27673
Zn1–4Zn1	0.26204	Zn2–Ce1	0.31027
Zn1–4Zn3	0.26807	Zn2–6Zn3	0.33025
Zn1–4Zn2	0.27673	Zn3–6Zn1	0.26807
Zn1–Ce1	0.34299	Zn3–Ce1	0.30258
		Zn3–Zn3	0.30258
		Zn3–2Ce1	0.30258
		Zn3–2Zn3	0.30258
		Zn3–6Zn2	0.33025

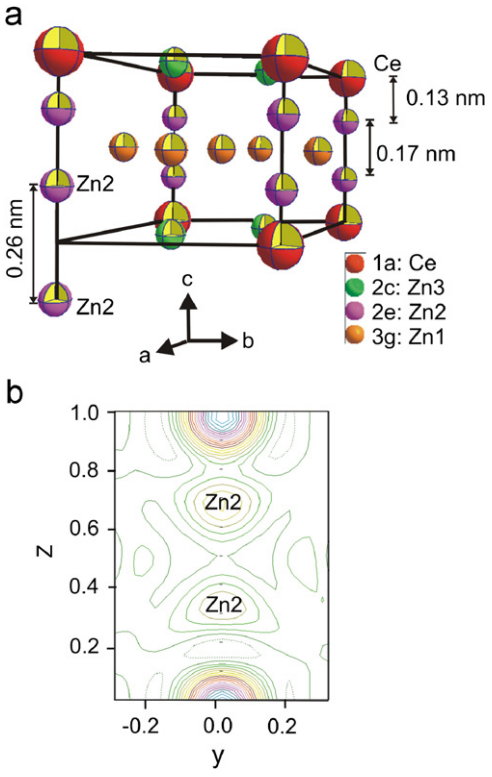

Fig. 4. (a) Crystal structure of hexagonal $CeZn_7$ [$Ce_{1-x}Zn_{5+2x}$ ($x=0.33$)] with $TbCu_7$-type. A Zn-dumbbell replaces the Ce-atom site in the left lower front corner. (b) Fourier map for hexagonal $CeZn_7$ projected onto the yz plane revealing the Zn-dumbbells.

3.2.2. The phase diagram Ce–Zn

Knowledge on the binary Ce–Zn phase diagram is summarized in two recent critical assessments and Calphad-type thermodynamic modelings of the binary system [11,12], both relying on the experimental solidus and liquidus data and the reaction isotherms determined by Chiotti and Mason [26]. In accordance with the published Ce–Zn phase diagram our X-ray reinvestigation confirmed the existence of all compounds hitherto reported. For a listing of crystal data of compounds (unit cell parameters, space group and structure type) see Table 1. Whereas the crystal structures of $CeZn_{11}$, $CeZn_5$, $CeZn_3$, $CeZn_2$ and CeZn, were found to be consistent with data in the literature (Table 1), precise structural data on atom site distribution, atom order and defect formation were provided for *hexagonal*-$CeZn_7$, Ce_3Zn_{22}, $Ce_{13}Zn_{58}$, and Ce_3Zn_{11} (for details see Section 3.2.1). We also confirm the irreversible character of the transition (about 750–800 °C on heating) between the low temperature form $CeZn_7$ ($Ce_{10}Zn_{90}$ at%) and the high temperature form βCe_2Zn_{17} ($Ce_{10.6}Zn_{89.4}$ at%), both existing at practically identical composition. Once βCe_2Zn_{17} has formed it is impossible to revert to $\alpha CeZn_7$ (αCe_2Zn_{17}), an observation already reported in earlier studies [21].

Evaluation of homogeneity regions of the binary compounds with respect to lattice parameter and EPMA data generally confirmed the various Ce-zincides as practically line-compounds without significant phase regions. Fig. 5 documents the two-phase regions for the boundary phases. There was no difference between the refined and reported lattice parameters of Zn [27] suggesting no solubility of Ce in Zn.

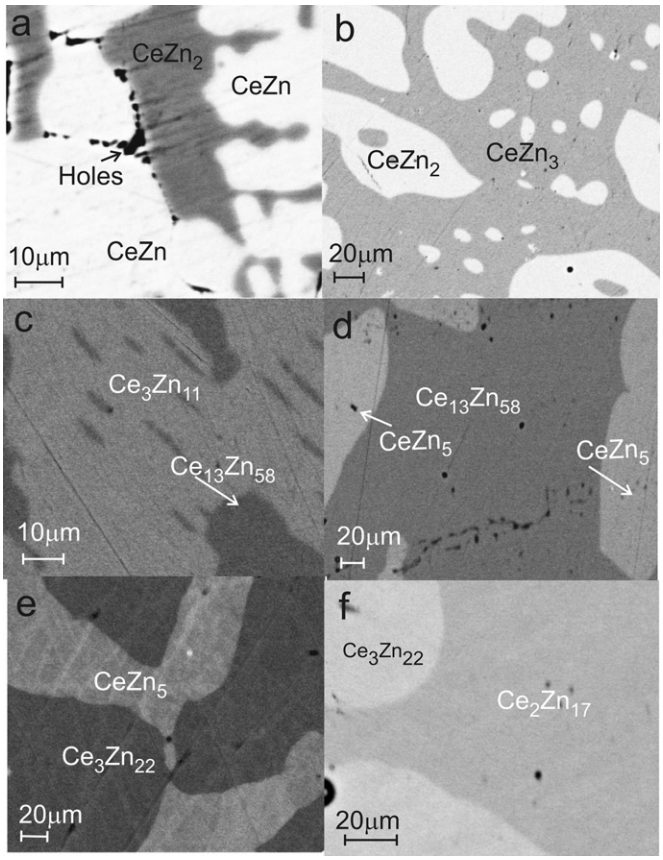

Fig. 5. Microstructures for selected Ce-Zn samples annealed at 800 °C for 7 days: (a) 40 at.%Ce, (b) 29 at.% Ce, (c) 20 at% Ce, (d) 17.6 at%, (e) 14.3 at.% Ce and (f), 11.27 at.% Ce.

3.3. The system Ce–Zn–B (< 50 at% Ce)

About 20 ternary alloys were prepared and analyzed by X-ray powder diffraction combined with EPMA. The analysis of the isothermal section at 800 °C did not reveal the formation of ternary compounds and all three-phase equilibria derived are documented in Table 4. Two-phase equilibria between Ce_xZn_y binaries and CeB_4 range from CeZn to Ce_3Zn_{22}, whereas Ce_2Zn_{17} and $CeZn_{11}$ tie to CeB_6 (see Fig. 6). In order to verify the equilibria a set of samples was made from CeB_6+$CeZn_x$ master alloys, which on formation of CeB_4 for ($2 < x < 7$) confirmed the triangulation in Fig. 6. Rietveld refinements of representative alloys are summarized in Fig. 7 and document that no ternary Ce–Zn–borides were observed in

Table 4
Phase analyses (EPMA and XPD) of Ce–Zn–B alloys, annealed at 800 °C.

Code	Nominal composition Ce–Zn–B (at%)	Experimental	Phase	Space group	Structure type	Lattice parameters (nm)		
						a	*b*	*c*
a	8–72–20	Ce_xB_y	$CeZn_{11}$	$I4_1/amd$	$BaCd_{11}$	1.06589(6)	–	0.68602(9)
		(ArcMelted)+	Ce_2Zn_{17}	$R\bar{3}m$	Th_2Zn_{17}	0.908727(6)	–	1.32822(1)
		Zn	CeB_6	$Pm\bar{3}m$	CaB_6	0.4149(1)	–	
b	17–50–33	Ce_xB_y	Ce_3Zn_{22}	$I4_1/amd$	Ce_3Zn_{22}	0.89339(2)	–	2.13793(6)
		(ArcMelted)+	$CeZn_5$	$P6/mmm$	$CaCu_5$	0.541078(9)	–	0.42778(1)
		Zn	CeB_4	$P4/mbm$	UB_4	0.72085(1)	–	0.409173(8)
c	19–45–36	Ce_xB_y	$CeZn_5$	$P6/mmm$	$CaCu_5$	0.541716(7)	–	0.427091(8)
		(ArcMelted)+	$Ce_{13}Zn_{58}$	$P6_3/mmc$	$Gd_{13}Cd_{58}$	1.46306(9)	–	1.4171(1)
		Zn	CeB_4	$P4/mbm$	UB_4	0.72076(1)	–	0.409129(8)
d	20–70–10	CeB_6	$Ce_{13}Zn_{58}$	$P6_3/mmc$	$Gd_{13}Cd_{58}$	1.46278(2)	–	1.4163(2)
		(ArcMelted)+	Ce_3Zn_{11}	$Immm$	La_3Al_{11}	0.45210(2)	0.88854(5)	1.34685(8)
		Ce_xZn_y	CeB_4	$P4/mbm$	UB_4	0.7209(1)	–	0.4048(1)
e	22–69–9	CeB_6	Ce_3Zn_{11}	$Immm$	La_3Al_{11}	0.45260(2)	0.89027(4)	1.34753(7)
		(ArcMelted)+	$CeZn_3$	$Cmcm$	$CeZn_3$	0.46338(4)	1.0460(1)	0.66440(6)
		Ce_xZn_y	CeB_4	$P4/mbm$	UB_4	0.72564(4)	–	0.40312(4)
f	28–62–10	CeB_6	$CeZn_3$	$Cmcm$	$CeZn_3$	0.46352(7)	1.0457(2)	0.6650(1)
		(ArcMelted)+	$CeZn_2$	$Imma$	$CeCu_2$	0.4673(1)	0.7512(8)	0.7557(1)
		Ce_xZn_v	CeB_4	$P4/mbm$	UB_4	0.7207(6)	–	0.4090(6)
		Unreacted	CeB_6	$Pm\bar{3}m$	CaB_6	0.41418(2)	–	–
g	43–37–20	CeB_4	$CeZn_2$	$Imma$	$CeCu_2$	0.46422(3)	0.75427(6)	0.75080(6)
		(ArcMelted)+	CeZn	$Pm\bar{3}m$	CsCl	0.37087(2)	–	–
		Ce_xZn_y	CeB_4	$P4/mbm$	UB_4	0.72022(6)	–	0.40860(6)

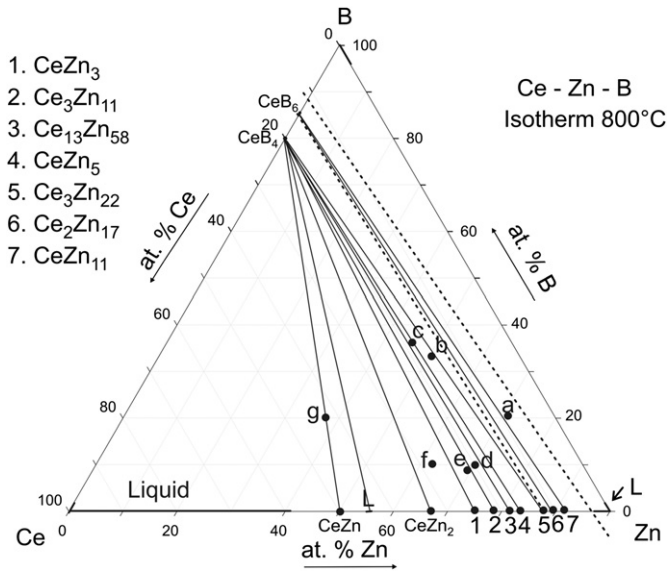

Fig. 6. Ce-Zn-B. Isothermal section at 800 °C.

the alloys investigated. It is, however, still unclear whether Ce_2Zn_{17} ties to CeB_4 or Ce_3Zn_{22} ties to CeB_6 (dashed line in Fig. 6).

In analogy to carbon incorporation in the Th_2Zn_{17} type structure of $Pr_2Mn_{17}C_{3-x}$ [28] we tested the solubility of boron as interstitial in Ce_2Zn_{17} for alloy $Ce_{8.6}Zn_{70.7}B_{20.7}$ (in at%). Rietveld refinement of the powder pattern, however, revealed no change in the lattice parameters with respect to binary Ce_2Zn_{17} as well as the absence of B in the octahedral voids [Ce_2Zn_4]. The interatomic distances $d_{B-Ce}=0.262$ and $d_{B-Zn}=0.189$ nm are unfavourable to form $Ce_2Zn_{17}B_{3-x}$. The evaluation of the Rietveld refinement is shown in Table 3a and Fig. 7d.

4. Conclusion

With EDX and WDX-electron microprobe analysis and X-ray powder diffraction we have derived the isothermal section for the system Ce–Zn–B at 800 °C. The section is characterized by the absence of ternary compounds and the absence of significant mutual solid solubilities of binary phases. In the course of the ternary system investigation the binary Ce–Zn system was re-evaluated on about 20 alloys. In the concentration range of

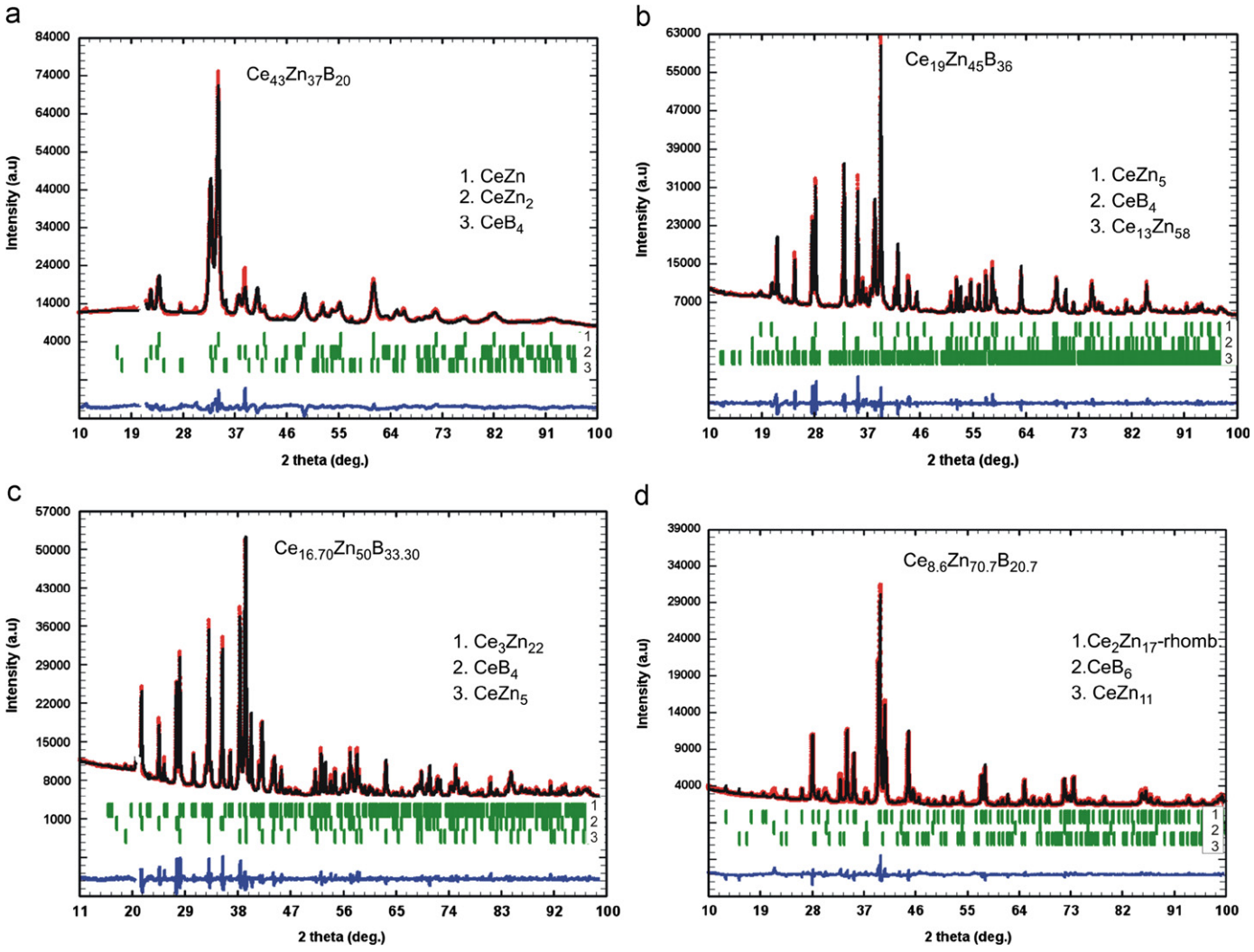

Fig. 7. Rietveld refinement for alloys (a) $Ce_{43}Zn_{37}B_{20}$, (b) $Ce_{19}Zn_{45}B_{36}$, (c) $Ce_{16.7}Zn_{50}B_{33.3}$ and (d) $Ce_{8.6}Zn_{70.7}B_{20.7}$. (Excluded regions in 7a ad c contain a small peak from sample holder).

10–10.5 at% Ce two structural modifications have been confirmed, which show irreversible transformation behaviour: high temperature βCe_2Zn_{17} exists above ~750 °C with the Th_2Zn_{17} type ($R\bar{3}m$, $a=0.90916(4)$ nm, $c=1.3286(1)$ nm) and low temperature $CeZn_7$ ($Ce_{1-x}Zn_{5+2x}$; $x\sim0.33$) adopts the $TbCu_7$ type (Rietveld refinement of X-ray powder data; $P6/mmm$, $a=0.52424(2)$, $c=0.44274(1)$ nm), which irreversibly transfers to the hT phase on heating above 750 °C. X-ray single crystal refinements have been carried out for several compounds, for which crystal structure data hitherto have only been derived from X-ray diffraction photographs. Thus precise data on atom site distribution and positional parameters have been provided for Ce_3Zn_{11} ($Immm$, $a=0.45242(2)$, $b=0.88942(3)$ and $c=1.34754(4)$ nm) and Ce_3Zn_{22} ($I4_1/amd$, a=0.89363(2) and $c=2.1804(5)$ nm).

Acknowledgments

The research reported herein was supported by the Higher Education Commission of Pakistan (HEC) under the scholarship scheme "PhD in Natural & Basic Sciences from Austria". We thank to Dr. S. Puchegger for his expert assistance in EPMA measurements.

References

[1] S. Murphy, Wear 98 (1984) 151–161.
[2] X. Tao, G. Wenguan, G. Pinlin, Zhongguo Xitu Xuebao 16 (3) (1998) 230–233.
[3] A.G..De Golyer, United State Patent Office. 1490696, 1923.
[4] I.J. Polmear, Light Alloys, third ed., Arnold, London, 1995.
[5] T. Roisnel, J. Rodriguez-Carvalaj, Mater. Sci. Forum 118 (1) (2010) 378–381.
[6] Nonius Kappa C.C.D. Program Package COLLECT, DENZO, SCALEPACK, SORTAV, Nonius Delft, The Netherlands, 1998.
[7] G.M..Sheldrick, SHELXS-97, Program for Crystal Structure Refinement University of Göttingen, Germany Windows version by McArdle, Natl. Univ. Ireland, Galway, 1997.
[8] G.M. Sheldrick, Acta Crystallogr. A64 (2008) 112–122.
[9] L.J. Farrugia, J. Appl. Crystallogr. 32 (1999) 837–838.
[10] T.B. Massalski, Binary Alloy Phase Diagrams, second ed., ASM International, Materials Park, OH, 1990.
[11] P.J. Spencer, A.D. Pelton, Y.-B. Kang, P. Chartrand, C.D. Fuerst, Calphad 32 (2008) 423–431.
[12] C.P. Wang, X. Chen, X.J. Liu, F.S. Pan, K. Ishida, J. Alloys Compd. 458 (2008) 166–173.
[13] P. Villars, K. Cenzual, Pearson's Crystal Data-Crystal Structure Database for Inorganic compounds (on CD-ROM), Release, ASM International, Materials Park, Ohio, USA, 2010/11.
[14] H. Okamoto, Desk Handbook: Phase Diagram for Binary Alloys, ASM International, Materials Park, OH, 2000.
[15] O. Zelinska, M. Conrad, B. Harbrecht, Z. Kristallogr., NCS 219 (2004) 357–358.
[16] B.G. Lott, P. Chiotti, Acta Crystallogr. 20 (1966) 733–738.
[17] P.I. Kripyakevich, Y.B. Kuz'ma, N.S. Ugrin, J. Struct. Chem., Translated from Zhural Strukturnoi Khimmi 8 (1967) 632–633.
[18] Q. Johnson, D.H. Wood, G.S. Smith, Acta Crystallogr. B24 (1968) 480–484.
[19] S. Piao, C.P. Gomez, S. Lidin, Z. Kristallogr. 221 (2006) 391–401.
[20] E. Veleckis, C.L. Rosen, H.M. Feder, J. Phys. Chem. 65 (1965) 2127–2131.
[21] A. Iandelli, A. Palenzona, J, Less-Common Metals 12 (1967) 333–343.
[22] T. Siegrist, Y.L. Page, J, Less-Common Metals 127 (1987) 189–197.
[23] E. Veleckis, R.V. Schablaske, I. Johnson, H.M. Feder, Trans. Metal. Soc. AIME 239 (1967) 58–63.
[24] K.H.J. Buschow, A.S. Van der Goot, Acta Crystallogr. B27 (1971) 1085–1088.
[25] R. Cerny., Y. Filinchuk, S. Brühne, Intermetallics 17 (2008) 818–825.
[26] P. Chiotti, J.T. Mason, Trans. Metal. Soc. AIME 233 (1965) 786–795.
[27] R.W. Lynch, H.G. Drickamer, J. Phy. Chem. Solids 26 (1965) 36–38.
[28] G. Block, W. Jeitschko, Inorg. Chem. 25 (1986) 279–282.
[29] M.M. Korsukova, V.N. Gurin, Y.B. Kuz'ma, A.Y. Kiskachi, N.E. Solov'ev, Sov. Phys. Crystallogr. 22 (6) (1977).
[30] Y.B. Kuz'ma, V.N. Gurin, M.M. Korsukova, A.L.G. Akselrud, Inorganic Mater., Izvestiya Akademii Nauk SSSR 23 (1987) 500–503.
[31] E. Parthé, L. Gelato, B. Chabot, M. Penzo, K. Censual, R. Gladyshevskii, TYPIX—Standardized Data and Crystal Chemical Characterization of Inorganic Structure Types, Springer, Berlin, 1994.